

Dark vertical conductance of cavity-embedded semiconductor heterostructures

Cassia Naudet-Baulieu,¹ Nicola Bartolo,¹ Giuliano Orso,¹ and Cristiano Ciuti¹

¹*Laboratoire Matériaux et Phénomènes Quantiques,
Université Paris Diderot, CNRS-UMR7162, 75013 Paris, France*

We present a linear-response nonlocal theory of the electronic conductance along the vertical (growth) direction of a generic doped semiconductor heterostructure embedded in a single-mode cavity electromagnetic resonator in the absence of illumination. The conductance depends on the ground-state properties and virtual collective polaritonic excitations that have been determined via a bosonic treatment in the dipole gauge. We show that, depending on the system parameters, the cavity vacuum effects can enhance or reduce significantly the dark vertical conductance with respect to the bare heterostructure.

I. INTRODUCTION

Semiconductor heterostructures like quantum wells (QW) and superlattices are the building blocks of important optoelectronic devices working in the mid and far infrared, such as photodetectors [1, 2] and quantum cascade lasers [3]. In the case of infrared photodetectors, the photo-induced vertical electrical current along the growth direction of the heterostructure is the key detected quantity. The sensitivity of a photodetector is limited by the so-called dark current, i.e. the current without illumination [2]. Several experimental and theoretical studies have investigated such systems [4–6], pointing out that the main origin of the dark current at low temperatures is the electron tunneling through potential barriers [7]. Recently, an improvement of the performances of Quantum-Well Infrared Photodetectors (QWIP) has been demonstrated for arrays of heterostructures embedded in photonic resonators [8].

Recent transport experiments in cavity-embedded organic semiconductors [9, 10] and in-plane magnetotransport measurements in cavity-embedded high-mobility two-dimensional electron systems [11] have shown that the linear-regime electronic conductance of a material can be significantly affected by a cavity electromagnetic resonator even in the absence of illumination. Early theoretical works exploring the role of a cavity on transport have focused on cavity-modified excitonic linear transport [12, 13] and charge nonlinear conduction [14] for chains of two-level systems in the nonlinear regime where electrons are injected in the excited levels. A recent theoretical work [15] on in-plane magnetotransport in the presence of Landau electronic levels has shown how virtual polariton excitations can control the charge transport in the linear regime. Indeed, light-matter interaction can play a pivotal role in determining the electronic transport properties without illumination especially if the strong or ultra-strong coupling regime [16] is achieved.

In this paper, we report a theoretical study of the electronic linear-regime conductance without illumination of a generic doped semiconductor heterostructure embedded in a cavity electromagnetic resonator at low temperature. By considering a nonlocal linear-response Kubo approach [17] and by determining the effective bosonic Hamilto-

nian for light-matter excitations, we calculate the system vertical conductance as a function of the system ground state and polaritonic excitations. In order to describe the collective electronic effects, we consider the system Hamiltonian in the dipole gauge [18–20] where two interaction terms emerge, describing respectively the so-called depolarization shift and the light-matter coupling. The present general framework is applied to quantum well heterostructures. Numerical results showing how the dark conductance is controlled by the cavity without illumination are presented.

The article is organized as follows. In Sec. II, we introduce the general theoretical bosonic framework to determine collective light-matter excitations. In Sec. III, within a many-body nonlocal Kubo formalism we provide the general expression for the dark vertical conductance for doped heterostructures depending on the properties of the ground state and of the polariton excitations. Numerical results for specific heterostructures are presented and discussed in Sec. IV. Finally, we draw our conclusions and perspectives in Sec. V. The most technical details about the theoretical model are reported in Appendix A and B.

II. HAMILTONIAN FRAMEWORK AND COLLECTIVE LIGHT-MATTER STATES

The system considered here is an arbitrary semiconductor heterostructure epitaxially grown along the z direction and embedded in a single-mode electromagnetic cavity. Single-mode electromagnetic resonators with tunable frequency can be obtained, for example, via LC-like structures [21–24] (see Fig. 1). We assume the electrons to be free in the transverse direction where $S = L_x \times L_y$ is the transverse area. The single-particle electronic eigenfunctions can be written as

$$\varphi_{j,\mathbf{q}}(\mathbf{r}) = \frac{e^{i\mathbf{q}\cdot\mathbf{r}_{\parallel}}}{\sqrt{S}}\phi_j(z), \quad (1)$$

where $\mathbf{r}_{\parallel} = \{x, y\}$ is the in-plane electron position and $\mathbf{q} = \{k_x, k_y\}$ the in-plane wavevector. The eigenfunctions ϕ_j and their energies E_j , are found by solving the one-dimensional Schrödinger equation for the motion along z ,

namely [25]:

$$\left(-\frac{\hbar^2}{2m_\star} \frac{\partial^2}{\partial z^2} + V(z)\right) \phi_j(z) = E_j \phi_j(z) \quad (2)$$

with m_\star the effective mass and $V(z)$ the potential describing an heterostructure of arbitrary shape. The in-plane energy dispersion of the state $\varphi_{j,\mathbf{q}}$ is $E_{j,\mathbf{q}} = E_j + \hbar^2 q^2 / (2m_\star)$. In the second quantization framework, it is convenient to introduce the fermionic operators $\hat{c}_{j,\mathbf{q}}$ ($\hat{c}_{j,\mathbf{q}}^\dagger$) which annihilate (create) an electron in the j -th band with wave-vector \mathbf{q} . In the absence of interactions, the many-body ground state is a Fermi sea with only the first j_F subbands populated, namely:

$$|\text{FS}\rangle = \prod_{j \leq j_F} \prod_{k < k_{Fj}} \hat{c}_{j,\mathbf{k}}^\dagger |\text{vacuum}\rangle, \quad (3)$$

where $k = |\mathbf{k}|$, k_{Fj} is the Fermi wave vector associated to the j -th band, while $|\text{vacuum}\rangle$ is the electronic and photonic vacuum. To describe the light-matter interaction for the heterostructure it is convenient to introduce collective electronic excitations [16, 19, 20] described by the operators

$$\hat{b}_{l,j}^\dagger = \frac{1}{\sqrt{N_{l,j}}} \sum_{\mathbf{q}} \hat{c}_{l,\mathbf{q}}^\dagger \hat{c}_{j,\mathbf{q}}, \quad (4)$$

for $j \leq j_F$ and $j < l$. The number $N_{l,j} = N_j - N_l > 0$ is the difference between the occupation numbers in the two conduction subbands and ensures the normalization of the state $\hat{b}_{l,j}^\dagger |\text{FS}\rangle$. To simplify the notation, we compact the double index l, j into $\nu = \{l, j\}$, assuming that any sum on such index runs over all the index pairs satisfying $l > j$ and $j \leq j_F$, unless differently specified. Note that in the limit where $N_\nu \gg 1$ the \hat{b}_ν operators satisfy bosonic commutation relations, that is $[\hat{b}_\nu, \hat{b}_{\nu'}^\dagger] = \delta_{\nu\nu'}$. In terms of the operators introduced in Eq. (4) and of the transition energies $\hbar\omega_\nu = E_l - E_j$, the free-electron part of the system Hamiltonian reads

$$\hat{\mathcal{H}}_e = \hbar \sum_{\nu} \omega_\nu \hat{b}_\nu^\dagger \hat{b}_\nu. \quad (5)$$

In the following, we wish to consider the Hamiltonian for an arbitrary semiconductor heterostructure embedded in a single-mode photonic cavity. Calling ω_c the frequency of the photon mode, the bare cavity contribution to the system Hamiltonian is given by

$$\hat{\mathcal{H}}_c = \hbar\omega_c \hat{a}^\dagger \hat{a}, \quad (6)$$

where \hat{a} (\hat{a}^\dagger) is the bosonic annihilation (creation) operator for a cavity photon.

To describe electromagnetic interactions, we will work here in the dipolar gauge [18, 19], giving rise to two interaction terms. The first describe the coupling between the cavity photon mode and the collective intersubband excitations:

$$\hat{\mathcal{H}}_{LM} = i\hbar (\hat{a}^\dagger - \hat{a}) \sum_{\nu} \Omega_\nu (\hat{b}_\nu^\dagger + \hat{b}_\nu), \quad (7)$$

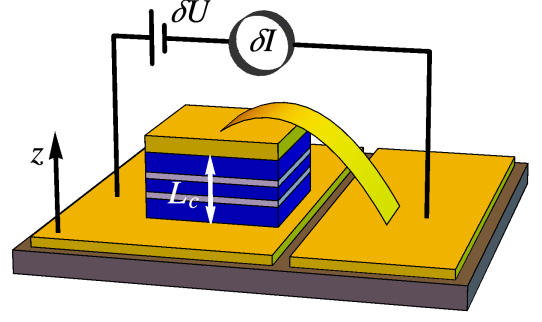


FIG. 1. Sketch of the considered system, namely a doped semiconductor heterostructure grown along the z direction and embedded in a single-mode photonic cavity of length L_c . The specific LC electromagnetic resonator here depicted is of the same type as in Ref. [24], where it is possible to tune the frequency of the cavity mode by changing the inductive bridge without altering the capacitive geometry of the cavity-embedded heterostructure. The key quantity analyzed in the present work is the vertical dark conductance $G = \delta I / \delta U$, where δI is the dark current (no illumination) and δU the voltage applied between the two leads separated by the cavity spacer length L_c .

where the collective vacuum Rabi frequency Ω_ν reads

$$\Omega_\nu = \sqrt{\frac{\hbar N_\nu e^2}{8\epsilon_0 \epsilon_r m_\star^2 S}} \sqrt{\frac{\omega_c}{L_c}} \frac{\int dz \xi_\nu(z)}{\omega_\nu} \quad (8)$$

with L_c the cavity length, $\epsilon_0 \epsilon_r$ the dielectric constant of the material filling the cavity, and

$$\xi_\nu(z) = [\partial_z \phi_l(z)] \phi_j(z) - \phi_l(z) [\partial_z \phi_j(z)]. \quad (9)$$

A relevant quantity indicating the strength of the light-matter coupling of a given transition is the resonant Rabi coupling $\Omega_\nu^{\text{res}} = \Omega_\nu|_{\omega_c = \omega_\nu}$. Note that the light-matter interaction Hamiltonian (7) includes both resonant and anti-resonant (counter-rotating wave) terms. The second interaction term is called depolarization shift Hamiltonian, which describes the self-interaction of the electronic polarization. In the considered system, it reads

$$\mathcal{H}_{dep} = \hbar \sum_{\nu} \sum_{\nu'} \Xi_{\nu\nu'} (\hat{b}_\nu^\dagger + \hat{b}_\nu) (\hat{b}_{\nu'}^\dagger + \hat{b}_{\nu'}), \quad (10)$$

where we have defined

$$\Xi_{\nu\nu'} = \frac{\hbar e^2}{8\epsilon_0 \epsilon_r m_\star^2 S} \frac{\sqrt{N_\nu N_{\nu'}}}{\omega_\nu \omega_{\nu'}} \int dz \xi_\nu(z) \xi_{\nu'}(z). \quad (11)$$

The depolarization Hamiltonian \mathcal{H}_{dep} is due to the collective part of the Coulomb interaction [26, 27]. The other Coulomb terms are responsible of non-collective electron-electron scattering which will be neglected here.

Finally, the total Hamiltonian reads

$$\hat{\mathcal{H}}_0 = \hat{\mathcal{H}}_e + \hat{\mathcal{H}}_c + \hat{\mathcal{H}}_{LM} + \hat{\mathcal{H}}_{dep}. \quad (12)$$

In this work, we will focus on the case where all the subbands $j \leq j_F$ are macroscopically occupied. In this limit, the collective excitations behave as bosons and the Hamiltonian (12) is quadratic in the bosonic operators \hat{a} and \hat{b}_ν . Hence, the eigenstates of the system can be determined by performing a Hopfield-Bogoliubov transformation [16, 27–29]. The Hamiltonian can be diagonalized by introducing the bosonic hybrid light-matter polaritonic annihilation operators

$$\hat{p}_r = w_r \hat{a} + y_r \hat{a}^\dagger + \sum_\nu \left(x_{r,\nu} \hat{b}_\nu + z_{r,\nu} \hat{b}_\nu^\dagger \right). \quad (13)$$

Indeed, in terms of such polariton operators, the total Hamiltonian (12) reads

$$\hat{\mathcal{H}}_0 = \hbar \sum_r \omega_r^I \hat{p}_r^\dagger \hat{p}_r. \quad (14)$$

The Hopfield-Bogoliubov coefficients and the polariton frequencies ω_r^I are determined by solving the eigenvalue equation $\mathbf{M} \vec{v}_r = \omega_r^I \vec{v}_r$, where the vector $\vec{v}_r = (w_r, x_{r,\nu_1}, x_{r,\nu_2}, \dots, y_r, z_{r,\nu_1}, z_{r,\nu_2}, \dots)^T$ and the matrix \mathbf{M} is given explicitly in Appendix A, Eq. (A1). To ensure the bosonic commutation relations $[\hat{p}_r, \hat{p}_{r'}^\dagger] = \delta_{r,r'}$, the coefficients must satisfy the hyperbolic normalization

$$|w_r|^2 - |y_r|^2 + \sum_\nu (|x_{r,\nu}|^2 - |z_{r,\nu}|^2) = 1. \quad (15)$$

III. DARK VERTICAL CONDUCTANCE

The goal of this section is to derive the dark vertical conductance of the cavity-embedded heterostructure, i.e. the linear-regime electronic transport along the growth direction without illumination. In order to do so, we first determine the nonlocal conductivity via a linear-response Kubo approach [17]. Specifically, we are interested in the linear response when a small bias voltage δU is applied along the vertical (growth) direction z between the two leads at the edges of the sample separated by the cavity spacer length L_c [cf. Fig. 1].

Assuming the heterostructure translationally invariant in the xy -plane, but not along the growth direction z , the electric field within the sample depends on z but not on \mathbf{r}_\parallel . The field in the z direction and the voltage are related by $E_z(z) = \partial_z U(z)$ with

$$\delta U = \int_{-L_c/2}^{L_c/2} dz E_z(z) = U(L_c/2) - U(-L_c/2). \quad (16)$$

The variation of current density in the low-temperature limit is determined through the non-local response function $\chi(z, z')$ via

$$\delta \langle \hat{J}_z \rangle(z) = \int_{-L_c/2}^{L_c/2} dz' \chi(z, z') E_z(z'), \quad (17)$$

with

$$\chi(z, z') = 2\hbar S \sum_{b>1} \frac{\eta_b}{\mathcal{E}_b - \mathcal{E}_1} \frac{\langle \Psi_1 | \hat{J}_z^\nabla(z) | \Psi_b \rangle \langle \Psi_b | \hat{J}_z^\nabla(z') | \Psi_1 \rangle}{(\mathcal{E}_b - \mathcal{E}_1)^2 + \eta_b^2}, \quad (18)$$

where $\{|\Psi_b\rangle\}_{b=1,2,\dots}$ are the many-body ground ($b=1$) and excited ($b>1$) states of the system considered, being \mathcal{E}_b the corresponding energies. The quantity $\eta_b = \hbar/\tau_b$ depends on the phenomenological scattering time τ_b [17, 30]. For purely electronic excitations, τ_b corresponds to the Drude transport scattering time τ_0 . Finally, the operator $\hat{J}_z^\nabla(z)$ is obtained from the z -component of the paramagnetic current density operator, upon integration on the transverse plane:

$$\hat{J}_z^\nabla(z) = i \frac{e\hbar}{2m_\star S} \sum_\nu \sqrt{N_\nu} \xi_\nu(z) (\hat{b}_\nu - \hat{b}_\nu^\dagger). \quad (19)$$

The formal derivation of Eqs. (17), (18), and (19) starting from the general Kubo formalism is detailed in Appendix B.

The derivation of the conductance from the two-point response function χ in non-translationally-invariant systems is a subtle task which has been addressed in detail for elastic scattering in disordered systems [31, 32]. The application of a bias δU across the sample induces a current δI coming out of the lead in $z = L_c/2$. The latter is related to the current density by $\delta I = S \delta \langle \hat{J}_z(L_c/2) \rangle$. After an integration by parts of Eq. (17), the current can be written as

$$\delta I = S [\chi(L_c/2, z) U(z)]_{-L_c/2}^{L_c/2} - S \int_{-L_c/2}^{L_c/2} dz' [\partial_{z'} \chi(L_c/2, z')] E(z'). \quad (20)$$

The term $\partial_{z'} \chi(L_c/2, z')$ contains the matrix elements of the operator $\partial_{z'} \hat{J}_z^\nabla(z')$. Using the definitions (19), (9), and the Schrödinger equation (2), one finds

$$\partial_{z'} \hat{J}_z^\nabla(z') = i \frac{e}{S} \sum_\nu \sqrt{N_\nu} \omega_\nu \phi_l(z') \phi_j(z') (\hat{b}_\nu^\dagger - \hat{b}_\nu). \quad (21)$$

The integral in Eq. (20) is a sum of terms proportional to

$$\sqrt{N_\nu} \omega_\nu \int_{-L_c/2}^{L_c/2} dz' \phi_l(z') \phi_j(z') E(z'), \quad (22)$$

which, in the limit of a slowly varying electric field, gives zero for any pair $\nu = \{l, j\}$. Within the considered formalism, we impose periodic boundary conditions in order to assure the continuity of the current [31]. Neglecting the integral term of Eq. (20), we finally obtain

$$\delta I = S \delta U \chi(L_c/2, L_c/2), \quad (23)$$

from which the general expression for the two-probe conductance is

$$G = \frac{\delta I}{\delta U} = S \chi(L_c/2, L_c/2). \quad (24)$$

As a result, we get

$$G = 2\hbar S^2 \sum_{b>1} \frac{\eta_b}{E_b - E_1} \frac{|\langle \Psi_1 | \hat{J}_z^\nabla(L_c/2) | \Psi_b \rangle|^2}{(E_b - E_1)^2 + \eta_b^2} \quad (25)$$

which is always a real and positive quantity.

A. Conductance for non-interacting electrons

Let us first consider the behavior of a non-interacting system (no light-matter interaction, no depolarization shift, i.e. $\hat{\mathcal{H}}_{LM} = \hat{\mathcal{H}}_{dep} = 0$). In this case $|\Psi_1\rangle = |\text{FS}\rangle$ and the only excited states connected to the ground state via $\hat{J}_z^\nabla(z)$ are $\hat{b}_\nu^\dagger |\text{FS}\rangle$, which are states containing a collective electron-hole excitation above the Fermi sea. This simplifies Eq. (18) to the form

$$\chi_{NI}(z, z') = \frac{\hbar n_e e^2}{2m_\star^2} \sum_\nu \frac{\tau_0}{\omega_\nu} \frac{\tilde{\xi}_\nu(z) \tilde{\xi}_\nu(z')}{1 + (\tau_0 \omega_\nu)^2}, \quad (26)$$

where $\tilde{\xi}_\nu(z) = \sqrt{N_\nu/N_e} \xi_\nu(z)$. The noninteracting conductance reads

$$G_{NI} = S \frac{\hbar n_e e^2}{2m_\star^2} \sum_\nu \frac{\tau_0}{\omega_\nu} \frac{|\tilde{\xi}_\nu(L_c/2)|^2}{1 + (\tau_0 \omega_\nu)^2}. \quad (27)$$

B. The cavity case: conductance in the absence of illumination

In presence of interaction with the cavity quantum field, we have a ground state $|\text{GS}\rangle \neq |\text{FS}\rangle$ and dressed polaritonic excited states defined by $\hat{p}_r^\dagger |\text{GS}\rangle$. The current operator (19) can be suitably rewritten exploiting the inverse of Eq. (13): $\hat{b}_\nu = \sum_r (x_{r,\nu}^* \hat{p}_r - z_{r,\nu} \hat{p}_r^\dagger)$. Thus, equation (18) can be easily applied to the new set of dressed manybody states to get

$$\chi(z, z') = \frac{\hbar n_e e^2}{2m_\star^2} \sum_r \frac{\tau_r}{\omega_r^I} \frac{\tilde{\xi}_r^{\text{eff}*}(z) \tilde{\xi}_r^{\text{eff}}(z')}{1 + (\tau_r \omega_r^I)^2} \quad (28)$$

with

$$\tilde{\xi}_r^{\text{eff}}(z) = \sum_\nu (x_{r,\nu} + z_{r,\nu}) \tilde{\xi}_\nu(z). \quad (29)$$

This finally gives the dark vertical conductance (i.e., in the absence of illumination)

$$G = S \frac{\hbar n_e e^2}{2m_\star^2} \sum_r \frac{\tau_r}{\omega_r^I} \frac{|\tilde{\xi}_r^{\text{eff}}(L_c/2)|^2}{1 + (\tau_r \omega_r^I)^2}. \quad (30)$$

Note that several effects contribute in determining how the cavity dark conductance (30) differs from the non-interacting one (27). First, the manybody ground and

excited states are dressed by the interactions, which can strongly modify the spatial localization of the manybody wavefunctions. This determines the spatial shape of $\tilde{\xi}_r^{\text{eff}}$ and is responsible for what we call the orbital renormalization of the conductance. Second, the interactions change the energetic cost associated to a polaritonic transition, thus altering the conductance. The third effect is the modification of the scattering times τ_r , which are associated to excited states having a mixed light-matter nature [15]. These hybrid scattering times are a weighted combination of the Drude electronic scattering time τ_0 and of a photonic transport scattering time τ_p :

$$\frac{1}{\tau_r} = \frac{W_{e,r}}{\tau_0} + \frac{1 - W_{e,r}}{\tau_p}, \quad (31)$$

where the electronic weight of the polariton created by p_r^\dagger is

$$W_{e,r} = \sum_\nu |x_{r,\nu}|^2 - \sum_\nu |z_{r,\nu}|^2. \quad (32)$$

Note that τ_p is not the photon lifetime inside the resonator, but a transport scattering time expected to be much longer [15]. In what follows, we will consider $\tau_p \gg \tau_0$, implying $\tau_r = \tau_0/W_{e,r}$.

C. Two-subband approximation

In general, there is a subtle interplay between orbital, energetic and scattering-time effects determining the conductance of a cavity-embedded heterostructure. One can get some analytical insight in the special case in which one transition gives a dominant contribution to the conductance. This is the case, for instance, when one transition frequency is significantly smaller than the others, since high-frequency terms are quickly suppressed in the sums of Eqs. (27) and (30). In this context, the four-by-four Hopfield-Bogoliubov matrix (A2) can be analytically diagonalized.

Let $\bar{\nu}$ be the two-component index associated to the dominant transition, the noninteracting conductance reads

$$G_{NI,\bar{\nu}} = S \frac{\hbar n_e e^2}{2m_\star^2} \frac{\tau_0}{\omega_{\bar{\nu}}} \frac{|\tilde{\xi}_{\bar{\nu}}(L_c/2)|^2}{1 + (\tau_0 \omega_{\bar{\nu}})^2}. \quad (33)$$

Making use of the exact relation

$$|x_{r,\bar{\nu}} + z_{r,\bar{\nu}}|^2 = W_{e,r} \frac{\omega_r^I}{\omega_{\bar{\nu}}}, \quad (34)$$

the cavity dark conductance can be recast as

$$G_{\bar{\nu}} = G_{NI,\bar{\nu}} \sum_{r=LP,UP} \frac{1 + (\tau_0 \omega_{\bar{\nu}})^2}{1 + (\tau_r \omega_r^I)^2}. \quad (35)$$

Note that in this one-transition approximation there are only two polaritonic branches: the lower ($r = LP$) and upper ($r = UP$) one.

Two relevant limits can be addressed. First, let us consider the limit $\omega_c \rightarrow 0$, where only the depolarization shift effect matters. In this case, we get

$$\begin{aligned} G_{\omega_c \rightarrow 0, \bar{\nu}} &= G_{NI, \bar{\nu}} \frac{1 + (\tau_0 \omega_{\bar{\nu}})^2}{1 + (\tau_0 \omega_{\bar{\nu}})^2 \left(1 + 4 \frac{\Xi_{\bar{\nu}}^2}{\omega_{\bar{\nu}}^2}\right)} \\ &\xrightarrow{\tau_0 \omega_{\bar{\nu}} \gg 1} \frac{G_{NI, \bar{\nu}}}{1 + 4 \frac{\Xi_{\bar{\nu}}^2}{\omega_{\bar{\nu}}^2}} \leq G_{NI, \bar{\nu}} \\ &\xrightarrow{\tau_0 \omega_{\bar{\nu}} \ll 1} G_{NI, \bar{\nu}}. \end{aligned} \quad (36)$$

The second limit is that of a high-frequency resonator: $\omega_c \rightarrow \infty$. The asymptotic value of the conductance reads

$$\begin{aligned} G_{\omega_c \rightarrow \infty, \bar{\nu}} &= G_{NI, \bar{\nu}} \frac{1 + (\tau_0 \omega_{\bar{\nu}})^2}{1 + (\tau_0 \omega_{\bar{\nu}})^2 \left[1 + 4 \left[\frac{\Xi_{\bar{\nu}}^2}{\omega_{\bar{\nu}}^2} - \left(\frac{\Omega_{\bar{\nu}}^{\text{res}}}{\omega_{\bar{\nu}}}\right)^2\right]\right]} \\ &\xrightarrow{\tau_0 \omega_{\bar{\nu}} \gg 1} \frac{G_{NI, \bar{\nu}}}{1 + 4 \left[\frac{\Xi_{\bar{\nu}}^2}{\omega_{\bar{\nu}}^2} - \left(\frac{\Omega_{\bar{\nu}}^{\text{res}}}{\omega_{\bar{\nu}}}\right)^2\right]} \leq G_{NI, \bar{\nu}} \\ &\xrightarrow{\tau_0 \omega_{\bar{\nu}} \ll 1} G_{NI, \bar{\nu}}. \end{aligned} \quad (37)$$

Note that one always has $\frac{\Xi_{\bar{\nu}}^2}{\omega_{\bar{\nu}}^2} \geq \left(\frac{\Omega_{\bar{\nu}}^{\text{res}}}{\omega_{\bar{\nu}}}\right)^2$ due to the Cauchy-Schwartz inequality

$$\int_{-L_c/2}^{L_c/2} dz \xi_{\bar{\nu}}^2(z) \geq \frac{1}{L_c} \left[\int_{-L_c/2}^{L_c/2} dz \xi_{\bar{\nu}}(z) \right]^2. \quad (38)$$

In the considered limits, since there is no scattering-time hybridization effect, the conductance modification is solely due to orbital and energetic effects. We see that the interactions always reduce the conductance with respect to the noninteracting case in the considered limits. It is also interesting to note that $G_{\omega_c \rightarrow 0, \bar{\nu}} \leq G_{\omega_c \rightarrow \infty, \bar{\nu}} \leq G_{NI, \bar{\nu}}$.

IV. NUMERICAL RESULTS FOR QUANTUM WELL STRUCTURES

In order to understand the impact of the cavity on the physical properties of the embedded heterostructure, we consider some paradigmatic examples. Let us start by studying a single quantum well whose potential barrier is V_0 and whose spatial width is L_{QW} , located at the middle of a cavity of length L_c .

A. Large cavity

First, we consider the case of a sample which has a cavity thickness L_c significantly larger than L_{QW} [Fig. 2(a)]. We set V_0 in order to have a single quantum confined state

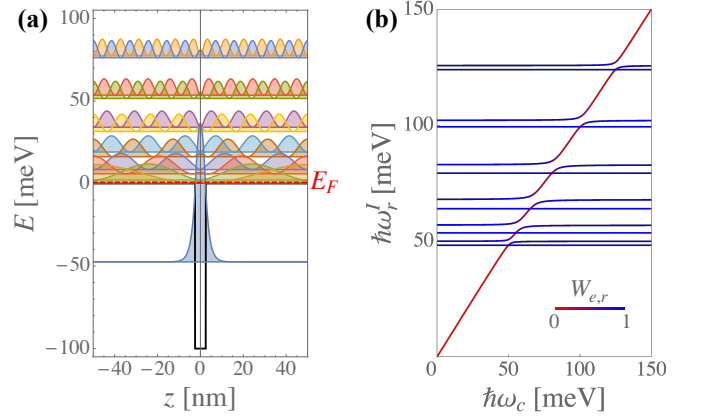


FIG. 2. Panel (a): single-electron energy levels and wavefunctions (square modulus, arbitrary units, offset vertically for clarity) for a cavity-embedded quantum well. System parameters: $V_0 = 100$ meV, $L_{QW} = 5$ nm, $L_c = 100$ nm, $m_* = 0.067 m_e$ with m_e the bare electron mass. Panel (b): energy spectrum of the polaritonic modes as a function of the cavity frequency for $n_e = 0.67 \times 10^{12} \text{ cm}^{-2}$, corresponding to a Fermi level energy E_F right below the pseudo-continuum [cf. Panel (a)]. In this specific configuration the largest polaritonic splitting at resonance corresponds to the $\nu = \{1, 5\}$ transition, with $\Omega_{\nu}^{\text{res}}/\omega_{\nu} \simeq 4.3\%$. Several other transitions happen to have similar coupling strengths. The curve color reflects the electronic (blue) or photonic (red) content of the polaritonic branch.

in the quantum well, followed by a quasi-continuum of states which are delocalized over the whole semiconductor region. Following the typical configuration of a QWIP, here we consider only electronic densities n_e such that the Fermi energy level is below the continuum threshold.

In Fig. 2(b) we present the polariton spectrum as a function of the cavity frequency ω_c . In order to maximize the light-matter coupling, we set $E_F = E_2$ [cf. panel (a)]. We can see that some “dark” states are completely uncoupled to the photonic mode, while the others show the typical anti-crossing behavior of polaritonic excitations. The region in which the polaritonic excitations manifests a hybrid light-matter nature is depicted in Fig. 2(b) via the color of the dispersion curve. The width of this region is proportional to the Rabi frequency $\Omega_{\nu}^{\text{res}}$.

For the same configuration of Fig. 2, the color map in Fig. 3 shows the cavity-embedded conductance G (normalized to $G_{\omega_c \rightarrow 0}$) as a function of the resonator frequency ω_c and of the doping density n_e . We can see sharp reductions of the conductance while changing the cavity mode frequency. These peaks match the occurrence of the polaritonic resonances observed in Fig. 2(b) and get wider when the light-matter coupling increases. This coincides with the region in which the polaritons get a hybrid light-matter nature. This effect is due to the scattering-time mixing [Eq. (31)]. Here the difference between $G_{\omega_c \rightarrow 0}$ and the noninteracting one G_{NI} (not shown in the plots) is negligible. This means that the orbital and energetic effects are minor for this considered case, which is dominated

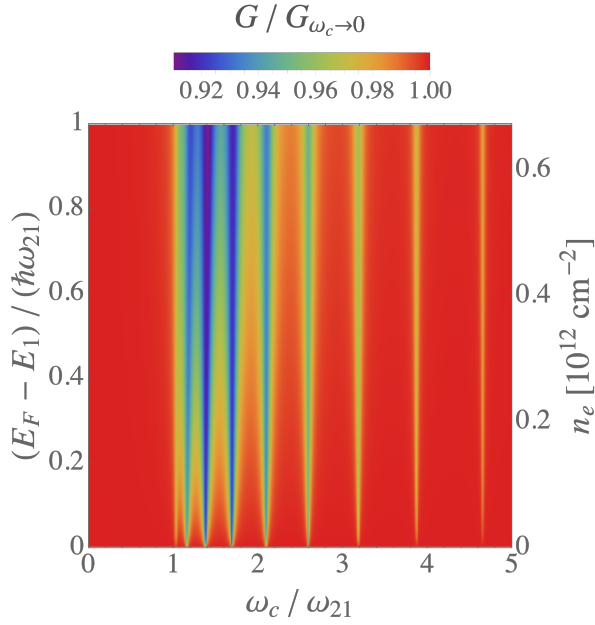


FIG. 3. Cavity conductance G (normalized to $G_{\omega_c \rightarrow 0}$) as a function of the cavity frequency ω_c (in units of the first transition frequency ω_{21}) and of the electronic density n_e . The maximum doping considered here corresponds to a Fermi energy level right below the quasi-continuum edge: $E_F = E_2$. Same parameters as in Fig. 2 and with Drude scattering time $\tau_0 = 1$ ps, corresponding to $\tau_0 \omega_{21} \simeq 70$. These results have been obtained including 80 subbands, which largely ensures convergence.

by the hybridization of the scattering times. For the considered parameters, the suppression of the conductance approaches 10%.

A critical parameter in determining the sign of the cavity-induced effects is the value of the Drude transport scattering time τ_0 . To elucidate its role, we show in Fig. 4 the ratio $G/G_{\omega_c \rightarrow 0}$ for the highest doping density (corresponding to $E_F = E_2$) and for different values of τ_0 . Generally, if the scattering time is long enough to have $\tau_0 \omega_{\nu} > 1$ we observe a suppression peak for $\omega_c \simeq \omega_{\nu}$, while the conductance is enhanced around resonances having $\tau_0 \omega_{\nu} < 1$. This confirms that, in the present configuration, the orbital renormalization is negligible and conductance is changed by the scattering-time mixing described by Eq. (31).

B. Thin cavity

In order to enhance the effects of the light-matter interaction on transport, one can reduce the cavity length L_c . In this way, there is a larger overlap between confined and delocalized wave functions, which tends to enhance both Ω_{ν} and Ξ_{ν}' . Furthermore, reducing L_c one automatically increases the resonant Rabi frequency $\Omega_{\nu}^{\text{res}} \propto L_c^{-1/2}$. A sketch of the considered system is presented in Fig. 5(a).

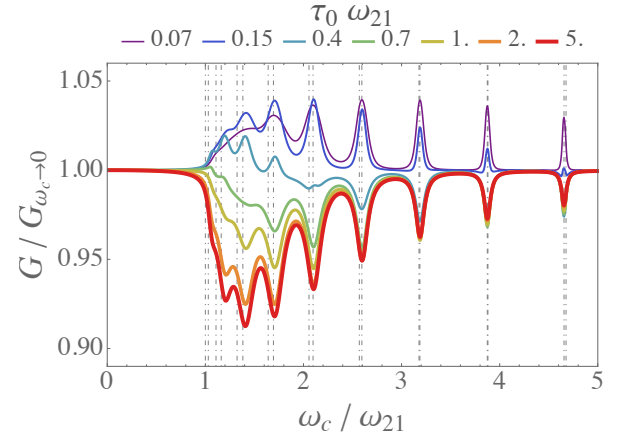


FIG. 4. Panel (a): same conductance ratio as in Fig. 3, but for a fixed value $n_e = 0.67 \times 10^{12} \text{ cm}^{-2}$ (i.e., $E_F = E_2$). Different curves correspond to different values of the Drude scattering time τ_0 (see legend). The behavior for $\tau_0 \omega_{21} > 5$ is practically unchanged with respect to red (thicker) curve. The vertical dot-dashed lines mark ω_{ν} for $\nu = \{1, n\}$ with $n = 2, 3, \dots$.

The parameters are the same as those of Fig. 2(a), except for $L_c = 20$ nm [33].

In Fig. 5(c) we show the effects of the interactions on the conductance for a Fermi energy level $E_F = E_2$, that is maximally-populating the confined subband only. We see that $G_{\omega_c \rightarrow 0}$ is smaller than the noninteracting one G_{NI} , with about a 10% reduction coming from the competition of orbital and energetic effects. The light-matter coupling induces resonances for coupled $1 \rightarrow n$ transitions and renormalizes the conductance for large ω_c . At the main resonance, the conductance reduction is approximately 32%.

When the Fermi level is raised in such a way to populate delocalized subbands, further transitions are allowed, giving significant contributions to the conductance. In Fig. 5(b) we show the different conductances for $E_F = E_4$. Here the depolarization shift reduces the conductance of almost one order of magnitude with respect to the noninteracting case. This large effect is smoothly renormalized by the light-matter coupling when the cavity frequency is increased. We still can observe residual effects of $2 \rightarrow n$ resonances, but in this configuration the scattering-time mixing is much less relevant than the orbital and energetic effects.

In this thin-cavity configuration, the energy subbands are sufficiently spaced for the two-subband approximation of Sec. III C to hold. The conductances in Fig. 5(d) have been obtained by restricting to the $2 \rightarrow 3$ transition for the configuration of Fig. 5(b). Similarly, Fig. 5(d) has been obtained considering the $1 \rightarrow 3$ transition for the configuration of Fig. 5(c). As we can see, the two-subband approximation captures rather well the physics. Remarkably, by increasing the cavity frequency the dark conductance increases by nearly an order of magnitude.

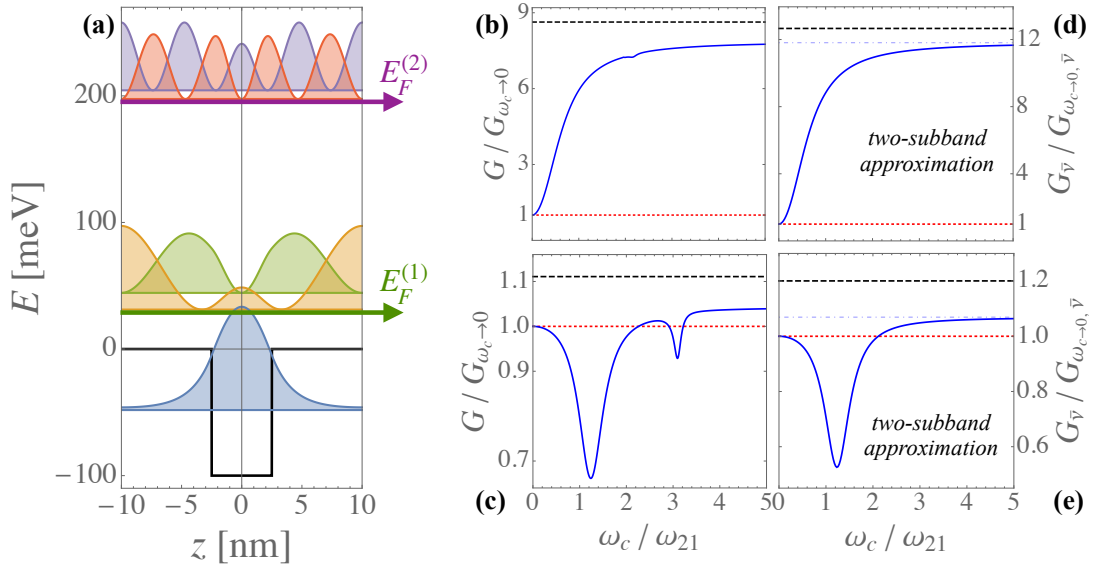


FIG. 5. Panel (a): same as Fig. 2(a), but for $L_c = 20$ nm. Panel (b-e): cavity conductance (normalized to the cavity-less limit $\omega_c \rightarrow 0$) as a function of ω_c/ω_{12} . The red dotted lines mark the reference cavity-less conductance, while the black dashed lines mark the noninteracting limit. Panel (c,e): results obtained for a Fermi energy level $E_F^{(1)} = E_2$, corresponding to a doping density $n_e = 1.1 \times 10^{12} \text{cm}^{-2}$. The main and dominant transition occurs for $\bar{\nu} = \{1, 3\}$ with $\hbar\omega_{\bar{\nu}} = 92.6$ meV, $\Omega_{\bar{\nu}}^{\text{res}} = 0.14\omega_{\bar{\nu}}$, $n_{\bar{\nu}} = n_e$, and $\Xi_{\bar{\nu}}^{\nu} = 0.05\omega_{\bar{\nu}}$. Panel (b,d): results obtained for $E_F^{(2)} = E_4$, corresponding to a doping density $n_e = 7.9 \times 10^{12} \text{cm}^{-2}$. The main and dominant transition occurs for $\bar{\nu} = \{2, 3\}$ with $\hbar\omega_{\bar{\nu}} = 13.2$ meV, $\Omega_{\bar{\nu}}^{\text{res}} = 1.7\omega_{\bar{\nu}}$, $n_{\bar{\nu}} = 0.18 \times 10^{12} \text{cm}^{-2}$, and $\Xi_{\bar{\nu}}^{\nu} = 2.92\omega_{\bar{\nu}}$. In Panels (b,c) we have used the full model including 80 conduction subbands. Panels (d,e) have been obtained within the two-subband approximation. In these panels, the blue dot-dashed lines mark the analytic asymptotic value $G_{\omega_c \rightarrow \infty, \bar{\nu}}/G_{\bar{\nu}}$. The Drude scattering time is $\tau_0 = 1$ ps.

V. CONCLUSIONS

In this work we have introduced a linear-response many-body formalism for the vertical conductance of an arbitrary doped semiconductor heterostructure. Within our formalism, it is possible to account for the effect of the light-matter coupling when such an heterostructure is embedded in a single-mode electromagnetic resonator in absence of illumination. We solved the many-body Hamiltonian in the dipole gauge, accounting for the collective Coulomb interaction (depolarization shift) and the light-matter coupling in a bosonized formalism. As summarized by Eq. (25), the conductance is controlled by virtual transitions from the manybody ground state to the excited states via the collective current operator \hat{J}_z^{∇} . The conductance depends on the matrix elements of the current operator between ground and polariton excited states, the energy of such polariton excitations as well as on the scattering times.

After presenting our general bosonized theory, we focused on the paradigmatic example of cavity-embedded quantum well heterostructures. We have shown that the cavity dark vertical conductance (no illumination) can be largely modified. This effect can be measured by observing the dependence of the conductance on the cavity mode frequency for a fixed cavity length L_c . The hybridization of the scattering times leads to the appearance of resonances in the conductance as a function of the cavity

frequency. These peaks can correspond to enhancement or suppression of the conductance depending on the value of the Drude electronic transport scattering time. Using parameters for *GaAs*-based semiconductor heterostructures, we have shown important effects both qualitatively and quantitatively. As possible future developments of the present theory, we mention the case of dispersive multimode cavities and the investigation of the regime where the number of electrons is not large enough to allow for a bosonic treatment of the elementary excitations.

Our findings are of pivotal importance for the understanding of electromagnetic-vacuum effects on the electronic transport of cavity-embedded systems. The flexibility of the formalism allows to apply our theory on any kind of heterostructure, which is all the more significant since several devices are based on this technology.

VI. ACKNOWLEDGMENTS

We thank A.D. Stone, R. Colombelli, J. Faist, C. Sirtori, G. Scalari, Y. Todorov for discussions.

Appendix A: Hopfield-Bogoliubov matrix for the considered system

The Hopfield-Bogoliubov matrix \mathbf{M} associated to the Hamiltonian (12) can be written in the following block form:

$$\mathbf{M} = \begin{pmatrix} \omega_c & -O & 0 & O \\ -O^\dagger & W + D & -O^\dagger & -D \\ 0 & O & -\omega_c & -O \\ -O^\dagger & D & -O^\dagger & -W - D \end{pmatrix} \quad (\text{A1})$$

with $O = (i\Omega_{\nu_1}, i\Omega_{\nu_2}, \dots)$, $W = \begin{pmatrix} \omega_{\nu_1} & & \\ & \omega_{\nu_2} & \\ & & \ddots \end{pmatrix}$ and

$$D = \begin{pmatrix} 2\Xi_{\nu_1}^{\nu_1} & 2\Xi_{\nu_1}^{\nu_2} & \dots \\ 2\Xi_{\nu_2}^{\nu_1} & 2\Xi_{\nu_2}^{\nu_2} & \dots \\ \vdots & \vdots & \ddots \end{pmatrix}.$$

When restricting to a single main transition of index $\bar{\nu}$, \mathbf{M} is a four by four matrix:

$$\mathbf{M} = \begin{pmatrix} \omega_c & -i\Omega_{\bar{\nu}} & 0 & i\Omega_{\bar{\nu}} \\ i\Omega_{\bar{\nu}} & \omega_{\bar{\nu}} + 2\Xi_{\bar{\nu}}^{\bar{\nu}} & i\Omega_{\bar{\nu}} & -2\Xi_{\bar{\nu}}^{\bar{\nu}} \\ 0 & i\Omega_{\bar{\nu}} & -\omega_c & -i\Omega_{\bar{\nu}} \\ i\Omega_{\bar{\nu}} & 2\Xi_{\bar{\nu}}^{\bar{\nu}} & i\Omega_{\bar{\nu}} & -\omega_{\bar{\nu}} - 2\Xi_{\bar{\nu}}^{\bar{\nu}} \end{pmatrix}. \quad (\text{A2})$$

Appendix B: Details about the linear-response formalism for the vertical nonlocal conductivity

In this Appendix we wish to show some intermediate steps of the derivation of Eqs. (17), (18), and (19) from a general linear-response function formalism. In the absence of external magnetic field and for an applied electric field E_z applied along the growth direction z , the current density variation in the sample is given by [17]

$$\delta\langle\hat{J}_z(\mathbf{r})\rangle = \int d^3\mathbf{r}' \tilde{\chi}(\mathbf{r}, \mathbf{r}') E_z(\mathbf{r}'). \quad (\text{B1})$$

The general nonlocal current-current response function $\tilde{\chi}(\mathbf{r}, \mathbf{r}')$ reads

$$\tilde{\chi}(\mathbf{r}, \mathbf{r}') = 2\hbar \sum_{exc} \frac{\eta_{exc}}{\mathcal{E}_{exc} - \mathcal{E}_{GS}} \frac{\langle\text{GS}|\hat{J}_z^\nabla(\mathbf{r})|exc\rangle\langle exc|\hat{J}_z^\nabla(\mathbf{r}')|\text{GS}\rangle}{(\mathcal{E}_{exc} - \mathcal{E}_{GS})^2 + \eta_{exc}^2}, \quad (\text{B2})$$

where $\hat{J}_z^\nabla(\mathbf{r})$ is the z -component of the paramagnetic current operator, namely

$$\hat{J}_z^\nabla(\mathbf{r}) = -i \frac{e\hbar}{2m_*} \left[\left(\partial_z \hat{\psi}^\dagger(\mathbf{r}) \right) \hat{\psi}(\mathbf{r}) - \hat{\psi}^\dagger(\mathbf{r}) \left(\partial_z \hat{\psi}(\mathbf{r}) \right) \right]. \quad (\text{B3})$$

In the formalism of second quantization on the basis of non-interacting one-electron wave functions (1), the current density operator reads

$$\hat{J}_z^\nabla(\mathbf{r}) = -i \frac{e\hbar}{2m_*} \sum_{i,j,\mathbf{k},\mathbf{q}} \xi_{i,j}(z) \frac{e^{i\mathbf{q}\cdot\mathbf{r}_\parallel}}{S} \hat{c}_{i,\mathbf{k}}^\dagger \hat{c}_{j,\mathbf{k}-\mathbf{q}}. \quad (\text{B4})$$

Since the heterostructure is translationally invariant in the xy -plane, the application of a bias voltage along z can only create a field $E_z(\mathbf{r}) = E_z(z)$. Similarly, the current variation $\delta\langle\hat{J}_z(\mathbf{r})\rangle$ can not depend on \mathbf{r}_\parallel . We can thus integrate over the transverse surface S both sides of Eq. (B1) and get

$$\delta\langle\hat{J}_z(z)\rangle = \int dz' \left[\frac{1}{S} \int d^2\mathbf{r}_\parallel \int d^2\mathbf{r}'_\parallel \tilde{\chi}(\mathbf{r}, \mathbf{r}') \right] E_z(z'). \quad (\text{B5})$$

The only dependence on \mathbf{r} and \mathbf{r}' of Eq. (B2) is in the current density operators. Hence, by introducing

$$\hat{J}_z^\nabla(z) \equiv \frac{1}{S} \int d^2\mathbf{r}_\parallel \hat{J}_z^\nabla(\mathbf{r}), \quad (\text{B6})$$

the term in square brackets in Eq. (B5) reads as $\chi(z, z')$ of Eq. (18), and Eq. (B5) becomes Eq. (17). Upon insertion of Eq. (B4) into Eq. (B6) one finally gets Eq. (19).

-
- [1] L. Gendron, M. Carras, A. Huynh, V. Ortiz, C. Koeniguer, and V. Berger, *Applied Physics Letters* **85**, 2824 (2004).
 - [2] C. Jagadish, S. Gunapala, and D. Rhiger, *Advances in infrared photodetectors*, Vol. 84 (Elsevier, 2011).
 - [3] J. Faist, F. Capasso, D. L. Sivco, C. Sirtori, A. L. Hutchinson, and A. Y. Cho, *Science* **264**, 553 (1994).
 - [4] B. F. Levine, C. G. Bethea, G. Hasnain, V. O. Shen, E. Pelve, and R. R. Abbott, *Applied Physics Letters* **56**, 851 (1990).
 - [5] A. Zussman, B. F. Levine, and J. Kuo, J. M. and De Jong, *Journal of Applied Physics* **70**, 5101 (1991).
 - [6] H. C. Liu, A. G. Steele, M. Buchanan, and Z. R. Wasilewski, *Journal of Applied Physics* **73**, 2029 (1993).
 - [7] B. F. Levine, *Journal of Applied Physics* **74**, R1 (1993).
 - [8] D. Palaferri, Y. Todorov, A. Bigioli, A. Mottaghizadeh, D. Gacemi, A. Calabrese, A. Vasanelli, L. Li, A. G. Davies, E. H. Linfield, F. Kapsalidis, M. Beck, J. Faist, and C. Sirtori, *Nature* **556**, 85 EP (2018).
 - [9] E. Orgiu, J. George, J. A. Hutchison, E. Devaux, J. F. Dayen, B. Doudin, F. Stellacci, C. Genet, J. Schachenmayer, C. Genes, G. Pupillo, P. Samorì, and T. W. Ebbesen, *Nature Materials* **14**, 1123 (2015).
 - [10] K. Nagarajan, J. George, A. Thomas, E. Devaux, T. Chervy, S. Azzini, J. Aziz, M. W. Hosseini, A. Kumar, C. Genet, and T. Ebbesen, *preprint ChemRxiv:7498622* (2018).
 - [11] G. L. Paravicini-Bagliani, F. Appugliese, E. Richter, F. Valmorra, J. Keller, M. Beck, N. Bartolo, C. Rössler,

- T. Ihn, K. Ensslin, C. Ciuti, G. Scalari, and J. Faist, *Nature Physics* **15**, 186 (2019).
- [12] J. Schachenmayer, C. Genes, E. Tignone, and G. Pupillo, *Phys. Rev. Lett.* **114**, 196403 (2015).
- [13] J. Feist and F. J. Garcia-Vidal, *Phys. Rev. Lett.* **114**, 196402 (2015).
- [14] D. Hagenmüller, J. Schachenmayer, S. Schütz, C. Genes, and G. Pupillo, *Phys. Rev. Lett.* **119**, 223601 (2017).
- [15] N. Bartolo and C. Ciuti, *Phys. Rev. B* **98**, 205301 (2018).
- [16] C. Ciuti, G. Bastard, and I. Carusotto, *Phys. Rev. B* **72**, 115303 (2005).
- [17] H. Bruus and K. Flensberg, *Many-Body Quantum Theory in Condensed Matter Physics* (Oxford, 2004).
- [18] M. Babiker and R. Loudon, *Proceedings of the Royal Society A: Mathematical, Physical and Engineering Sciences* **385**, 439 (1983).
- [19] Y. Todorov and C. Sirtori, *Phys. Rev. B* **85**, 045304 (2012).
- [20] E. Cortese, I. Carusotto, R. Colombelli, and S. D. Liberato, *Optica* **6**, 354 (2019).
- [21] B. Lee, I.-M. Lee, S. Kim, D.-H. Oh, and L. Hesselink, *Journal of Modern Optics* **57**, 1479 (2010).
- [22] Y. Todorov and C. Sirtori, *Phys. Rev. X* **4**, 1031 (2014).
- [23] B. Paulillo, J. M. Manceau, A. Degiron, N. Zerounian, G. Beaudoin, I. Sagnes, and R. Colombelli, *Opt. Express* **22**, 21302 (2014).
- [24] B. Paulillo, S. Pirotta, H. Nong, P. Crozat, S. Guilet, G. Xu, S. Dhillon, L. H. Li, A. G. Davies, E. H. Linfield, and R. Colombelli, *Optica* **4**, 1451 (2017).
- [25] For simplicity, we neglect here the variation of effective mass along the heterostructure.
- [26] S.-C. Lee and I. Galbraith, *Phys. Rev. B* **59**, 15796 (1999).
- [27] S. De Liberato and C. Ciuti, *Phys. Rev. B* **85**, 125302 (2012).
- [28] J. J. Hopfield, *Phys. Rev.* **112**, 1555 (1958).
- [29] P. Nataf and C. Ciuti, *Nature communications* **1**, 72 (2010).
- [30] P. B. Allen, *Conceptual Foundations of Materials: A Standard Model for Ground- and Excited-State Properties*, edited by S. Louie and M. Cohen, Contemporary Concepts of Condensed Matter Science (Elsevier Science, 2006).
- [31] H. U. Baranger and A. D. Stone, *Phys. Rev. B* **40**, 8169 (1989).
- [32] C. L. Kane, R. A. Serota, and P. A. Lee, *Phys. Rev. B* **37**, 6701 (1988).
- [33] We point out that this thin cavity configuration is more challenging to measure experimentally since the resistance $1/G$ of the semiconductor heterostructure is smaller and in principle can become comparable to the resistance of ohmic contacts. We checked that, in the considered regime of parameters, the resistance $1/G$ is significant compared to typical resistances of ohmic contacts [34].
- [34] A. Baca, F. Ren, J. Zolper, R. Briggs, and S. Pearton, *Thin Solid Films* **308-309**, 599 (1997).